Hindawi
Journal of Nanotechnology
Volume 2022, Article ID 8947080, 10 pages
https://doi.org/10.1155/2022/8947080

Research Article

Electrochemically Effective Surface Area of a Polyaniline Nanowire-Based Platinum Microelectrode and Development of an Electrochemical DNA Sensor

Luyen Thi Tran, Hoang Vinh Tran, Ha Hong Cao, Thuy Hong Tran, and Chinh Dang Huynh

Hanoi University of Science and Technology, 1 Dai Co Viet Road, Hanoi 100000, Vietnam

Correspondence should be addressed to Luyen Thi Tran; luyen.tranthi@hust.edu.vn

Received 12 January 2022; Revised 25 April 2022; Accepted 26 April 2022; Published 17 May 2022

Academic Editor: Jorge M. Seminario

Electrochemical DNA sensors based on nanocomposite materials of polyaniline nanowires (PANi NWs) have been published in the literature. However, it is interesting that there are very few research studies related to the development of electrochemical DNA sensors based on PANi NWs individually. In this study, PANi NWs were synthesized site-specifically on a Pt microelectrode with only 0.785 mm^2 area using an electropolymerization procedure. The electrosynthesis allows direct deposition of PANi NWs onto the Pt microelectrode in a rapid and cost-effective way. The good properties of PANi NWs including uniform size, uniform distribution throughout the Pt working electrode, and H_2SO_4 doping which improved the conductivity of the PANi material were obtained. Especially, the electrochemically effective surface area of the PANi NW-based Pt microelectrode determined in this work is nearly 19 times larger than that of the Pt working electrode. The PANi NW layer with large electrochemically effective surface area and high biocompatibility is consistent with the application in electrochemical DNA sensors. The fabricated DNA sensors show advantages such as simple fabrication, direct detection, high sensitivity (with the detection limit of 2.48×10^{-14} M), good specificity, and low sample volume requirement. This study also contributes to confirm the role of PANi NWs in DNA probe immobilization as well as in electrochemical signal transmission in the development of electrochemical DNA sensors.

1. Introduction

DNA sensors have demonstrated a wide range of applications in detection of pathogenic viruses and bacteria, disease diagnosis, and food safety monitoring [1–5]. Particularly, electrochemical DNA sensors have shown many advantages such as high sensitivity, good selectivity, rapid detection time, reasonable cost, and high compatibility with lab-on-a-chip systems [6–8]. In the development of electrochemical DNA sensors, many studies have been carried out to improve the sensitivity of sensors, to simplify the sensor fabrication process, and to miniaturize the analytical system [9–11]. In these strategies, the microelectrode modification using nanostructured materials is an important solution that contributes to promoting the research and application of electrochemical DNA sensors [12–14].

Nanostructured conducting polymers with excellent properties, such as good electrical conductivity, environmental durability, ease of preparation, and ability to integrate with electronic components, are ideal materials for various applications including nanoelectronic devices, catalysts, electron field emitters, actuators, membranes, biomedical devices, rechargeable batteries, supercapacitors, sensors, and especially, electrochemical DNA sensors [15–20]. In the field of electrochemical DNA sensors, one-dimensional nanostructures of polyaniline (PANi) including PANi nanowires (PANi NWs), PANi nanotubes, PANi nanofibers, and PANi nanorods have attracted research interest due to their large surface area, tunable electrochemical properties, and high biocompatibility [21]. An electrochemical DNA sensor operates based on the principle that interactions between the probe and target DNA sequences will cause changes in the sensor's electrochemical

Table 1: The probe and target DNA sequences used in this work.

Probe	5′-AGACCTCCAGTCTCCATGGTACGTC-3′
Complementary target	5′-GACGTACCATGGAGACTGGAGGTCT-3′
Noncomplementary target	5′-ACGCTGAGTACGGGTGCAAGAGTCA-3′

signals. In the fabrication of electrochemical DNA sensors, the PANi nanomaterials can play important roles as intermediate material layers between DNA probe sequences and metal microelectrodes [22]. These PANi nanomaterials can act as linking agents for the immobilization of DNA probe sequences on the microelectrode surface and can enhance the signal transmission from biointeractions to transducers [22]. Therefore, the one-dimensional PANi nanostructures can be used to modify the microelectrode surface in order to fabricate electrochemical DNA sensors with high sensitivity [12, 23].

The one-dimensional PANi nanostructures can be fabricated using chemical and/or electrochemical routes [24–26]. In the development of electrochemical DNA sensors based on one-dimensional nanostructures, electrosynthesis methods have shown many advantages compared to chemical methods, such as rapidity, ease of mass production, uniformity, and low cost [27]. Besides, electrosynthesis methods allow one-dimensional nanostructures to grow directly on electrode surfaces, thereby overcoming the disadvantage of chemical methods, which is the difficulty in binding the synthesized nanomaterials with electrode surfaces [22]. Moreover, when using electrosynthesis methods, the size of one-dimensional nanostructures and the thickness of nanomaterial layers formed on electrode surfaces can be easily controlled by changing synthesis conditions [25, 28]. Therefore, the application of nanocomposite materials containing electrosynthesized PANi NWs in the fabrication of electrochemical DNA sensors has been published in the literature [12, 23, 29]. However, there are very few research studies related to the development of electrochemical DNA sensors based on PANi NWs individually.

In this work, PANi NWs were synthesized directly on a Pt microelectrode with only 0.785 mm^2 area using an electrochemical procedure. Electrochemically effective surface area of the Pt/PANi NW microelectrode, which is an important parameter affecting the sensitivity of an electrochemical sensor, was determined using data from electrochemical measurements. Then, a simple and effective electrochemical DNA sensor was developed using the optimized Pt/PANi NW microelectrode. The Pt/PANi NW microelectrode with unique structural and electrochemical properties was expected to simplify the DNA probe immobilization, to improve the electrochemical signals of the fabricated DNA sensor, and to reduce the volumes of analytical samples. This work will also contribute to confirm the role of PANi NWs in the development of electrochemical DNA sensors.

2. Experiment

2.1. Chemicals and Instrumentations

2.1.1. Chemicals. Aniline ($C_6H_5NH_2$, 99.5 wt.%), phosphate buffer solution (PBS), potassium hexacyanoferrate(III) ($K_3Fe(CN)_6$, 99 wt.%), potassium hexacyanoferrate(II) trihydrate ($K_4Fe(CN)_6.3H_2O$, 99.95 wt.%), and potassium chloride (KCl, 99 wt.%) were from Sigma Aldrich. The supporting chemicals including nitrogen (N_2, 99.9 wt.%), potassium dichromate ($K_2Cr_2O_7$, 99 wt.%), and sulfuric acid (H_2SO_4, 98 wt.%) were of analytical grade. The probe DNA strands and the complementary and noncomplementary target DNA strands provided by Integrated DNA Technologies (IDT) are shown in Table 1.

2.1.2. Integrated Pt Microelectrodes. The integrated Pt microelectrode consisting of a 0.785 mm^2 working electrode (WE) and a 5.0 mm^2 counterelectrode (CE) was deposited on a SiO_2/Si substrate using the cathode sputtering technique. Its configuration and fabrication process were discussed in our previous study [27]. The fabrication process is briefly described as follows: first, a silicon wafer was thermally oxidized to create an insulation oxide layer, and a photoresist layer was then coated on the surface of SiO_2; second, a photomask was placed onto a mask aligner and exposed to an UV light; third, the wafer was immersed in a development solution to remove undesired parts of photoresist, and then desired parts on the wafer were hardened by thermal annealing in the air. After that, the sputtering technique was applied to deposit a platinum membrane.

2.1.3. Instrumentations. A PGSTAT302N Autolab electrochemical workstation connected with an Ag/AgCl electrode in 3 M KCl solution (as a reference electrode, RE) and the fabricated Pt microelectrode (consisting of the WE and the CE) was used to perform electropolymerization of PANi NWs and to conduct electrochemical measurements. A Nova NanoSEM 450 microscope was used to investigate the surface morphology and chemical composition of PANi NWs through scanning electron microscopy (SEM) images and energy dispersive X-ray spectroscopy (EDX) spectra. A LabRAM HR 800 Raman was used to study the structural properties of PANi NWs.

2.2. Electropolymerization of PANi NWs on Pt Working Electrodes (WEs). An electrolyte solution containing 0.05 M aniline and 0.5 M H_2SO_4 was blown with N_2 gas for 15 minutes to remove the dissolved oxygen. The chronoamperometry (CA) method with an applied voltage of 0.9 V vs. Ag/AgCl RE was used to electropolymerize PANi NWs on the Pt WEs. After that, the Pt/PANi NW WEs were gently washed with deionized water and were dried at room temperature.

2.3. Immobilization of DNA Probe on Pt/PANi NW WEs and Detection of DNA Target Using PANi NW-Based Electrochemical DNA Sensors. Each of the Pt/PANi NW WEs was

coated with 5 μL of a DNA probe solution (10 μM in PBS, pH 7.4). The immobilization of DNA probe was kept for 2 hours at room temperature. The Pt/PANi NW/DNA probe microelectrodes were then washed with deionized water to remove DNA probe sequences with weak binding to PANi NWs and were dried at room temperature.

After that, each of the fabricated DNA sensors was dropped with 5 μL of complementary DNA target solution with different concentrations (from 1.0×10^{-13} M to 1.0×10^{-8} M) in PBS (pH 7.4). The DNA hybridization was conducted for 2 hours at room temperature. Then, electrochemical impedance spectroscopy (EIS) spectra of the DNA sensors were recorded in a solution consisting of $K_3Fe(CN)_6/K_4Fe(CN)_6$ (0.005 M) and 0.1 M·KCl in PBS (pH 7.4). The frequency range was from 10^5 Hz to 0.1 Hz, the AC potential was 5 mV, and the DC potential was 160 mV. In the EIS spectra, the increase in the electron transfer resistance ΔR_{ct} ($\Delta R_{ct} = R_{ct,i} - R_{ct,0}$), where $R_{ct,i}$ and $R_{ct,0}$ are the electron transfer resistances in the presence and absence of the DNA target, respectively, is used as the DNA hybridization signal.

3. Results and Discussion

3.1. Structural and Electrochemical Characterization of PANi NWs Electrosynthesized on Pt Microelectrodes. PANi NWs were electropolymerized directly on Pt WEs using the CA method. The CA curves recorded during these electropolymerization processes with different sets of time are shown in Figure 1(a). As can be seen in Figure 1(a), curve a–d, the current increases when the time for electropolymerization increases from 300 to 600 seconds. The maximum current value is obtained when the electropolymerization time is 600 seconds (Figure 1(a), curve d). The formation of conductive polymer layers with good electrical conductivity on Pt WEs led to the increase in the current density. The high current density would be favorable for signal transmission from the biological interaction to the transducer in the development of electrochemical DNA sensors. However, when the electropolymerization time continued to increase (higher than 600 seconds), it appeared that the formed PANi layer was too thick to adhere to the Pt WE's surface and was peeled off during the washing of the Pt/PANi NW electrode with deionized water. Therefore, the selected polymerization time for the subsequent electrosynthesis processes was 600 seconds.

The EIS spectra in Nyquist form of the Pt/PANi NW WEs recorded in $K_3Fe(CN)_6/K_4Fe(CN)_6$ (0.005 M) and 0.1 M KCl solution corresponding to the different electropolymerization times are also shown in Figure 1(b). In Figure 1(b), curve a–d, the charge transfer resistance (R_{ct}) value decreases from 1647 Ω (Figure 1(b), curve a) to 75 Ω (Figure 1(b), curve d) when the electropolymerization time increases from 300 to 600 seconds. The R_{ct} value is the smallest (75 Ω) when the electropolymerization time is 600 seconds (Figure 1(b), curve d). The EIS spectra in Figure 1(b) are completely consistent with the CA results in Figure 1(a). These EIS results further confirmed that the selected electropolymerization time of 600 seconds was appropriate.

Figure 1(c) shows the CV results of the Pt and Pt/PANi NW WEs measured in $K_3Fe(CN)_6/K_4Fe(CN)_6$ (0.005 M) and 0.1 M KCl solution. The Pt/PANi NW WE (Figure 1(c), curve b) has a higher peak current than the Pt WE (Figure 1(c), curve a). PANi NWs with high conductivity grew directly on the Pt WE; as a result, the peak current of the Pt/PANi NW WE increased. The use of highly electroactive PANi NWs to modify the Pt WE was expected to improve the electrochemical active area for DNA probe immobilization and to enhance the electrochemical signal of DNA sensors.

The SEM image of PANi NWs electrosynthesized on the Pt WE is shown in Figure 2(a). The average diameter of PANi NWs is 102 nm (Figure 2(b)). The size of PANi NWs is relatively uniform, and PANi NWs are distributed throughout the WE surface. The uniform distribution of PANi NWs on the WE surface will play an important role in enhancing the repeatability of electrochemical DNA sensors. The synthesized PANi material with nanowire structure will be more favorable for the DNA probe immobilization than the PANi film form [22, 30].

Figure 2(c) shows the Raman spectrum of PANi NWs formed on the Pt WE surface. The characteristic peaks for the PANi material are consistent with the descriptions in the literature. The band related to the C–H bending vibrations corresponding to the quinoid and benzenoid rings is at 1163 cm^{-1} [31]. The bands at 1257, 1352, and 1477 cm^{-1} are assigned to the C–N stretching mode of polaronic units, the $C–N^+$ vibration of polaronic structures, and the C=N stretching mode of the quinoid rings [12, 31, 32], respectively. The band associated with the C–C stretching mode of the benzenoid rings is at 1591 cm^{-1} [31]. Besides, the bands at 748, 783, 807, and 837 cm^{-1} are associated with the out-of-plane C–H motions which depend on the torsion angle between two aniline rings of the emeraldine form of PANi [32–34]. The Raman spectrum demonstrates that the PANi material was successfully electrosynthesized on the Pt WE and existed in the emeraldine form, which is the most conductive form of PANi.

The EDX spectrum of PANi NWs on the Pt WE is shown in Figure 2(d). Carbon and nitrogen elements observed at 0.27 and 0.39 keV are constituents of PANi NWs. On the other hand, the presence of oxygen and sulfur elements at 0.54 and 2.31 keV indicates that H_2SO_4 is doped into PANi NWs. The doping of PANi NWs with H_2SO_4 will play an important role in improving the conductivity of PANi NWs [35, 36]; thus, it will help to enhance the electrochemical signals of DNA sensors.

Electrochemically effective surface area (A) of WEs is an important factor that improves the electrochemical response and the sensitivity of electrochemical sensors [37]. In this study, the electrochemically effective surface area of the PANi NW-based Pt WE was determined by its CV data recorded at different potential scan rates from 30 to 80 $mV \cdot s^{-1}$ in $K_3Fe(CN)_6/K_4Fe(CN)_6$ (0.005 M) and

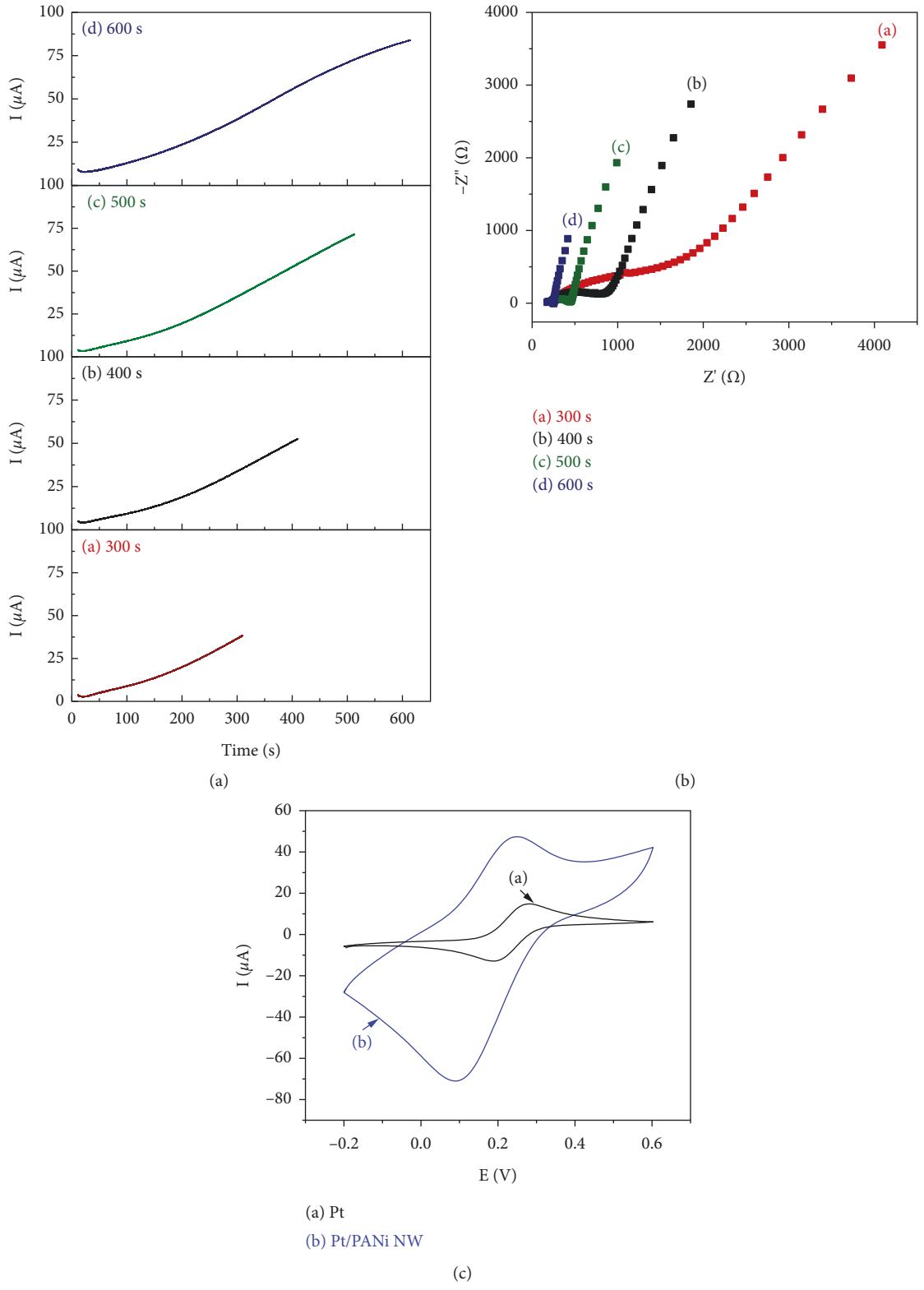

FIGURE 1: (a) Chronoamperometric curves during electropolymerization of PANi NWs on Pt WEs in 0.05 M aniline and 0.5 M H_2SO_4 with different sets of time: (a) 300, (b) 400, (c) 500, and (d) 600 seconds; (b) EIS spectra (Nyquist plots) of Pt/PANi NW electrodes in which PANi NWs were electrosynthesized with different sets of time: (a) 300, (b) 400, (c) 500, and (d) 600 seconds; and (c) CV results of (a) Pt and (b) Pt/PANi NW electrodes. Experimental conditions: EIS spectra were measured in $K_3Fe(CN)_6/K_4Fe(CN)_6$ (0.005 M) and 0.1 M KCl solution, frequency range: 100 kHz–100 mHz, $E_{AC} = 5$ mV, and $E_{DC} = 160$ mV; CV measurements were conducted at a scan rate of 50 mV s^{-1} in $K_3Fe(CN)_6/K_4Fe(CN)_6$ (0.005 M) and 0.1 M KCl solution.

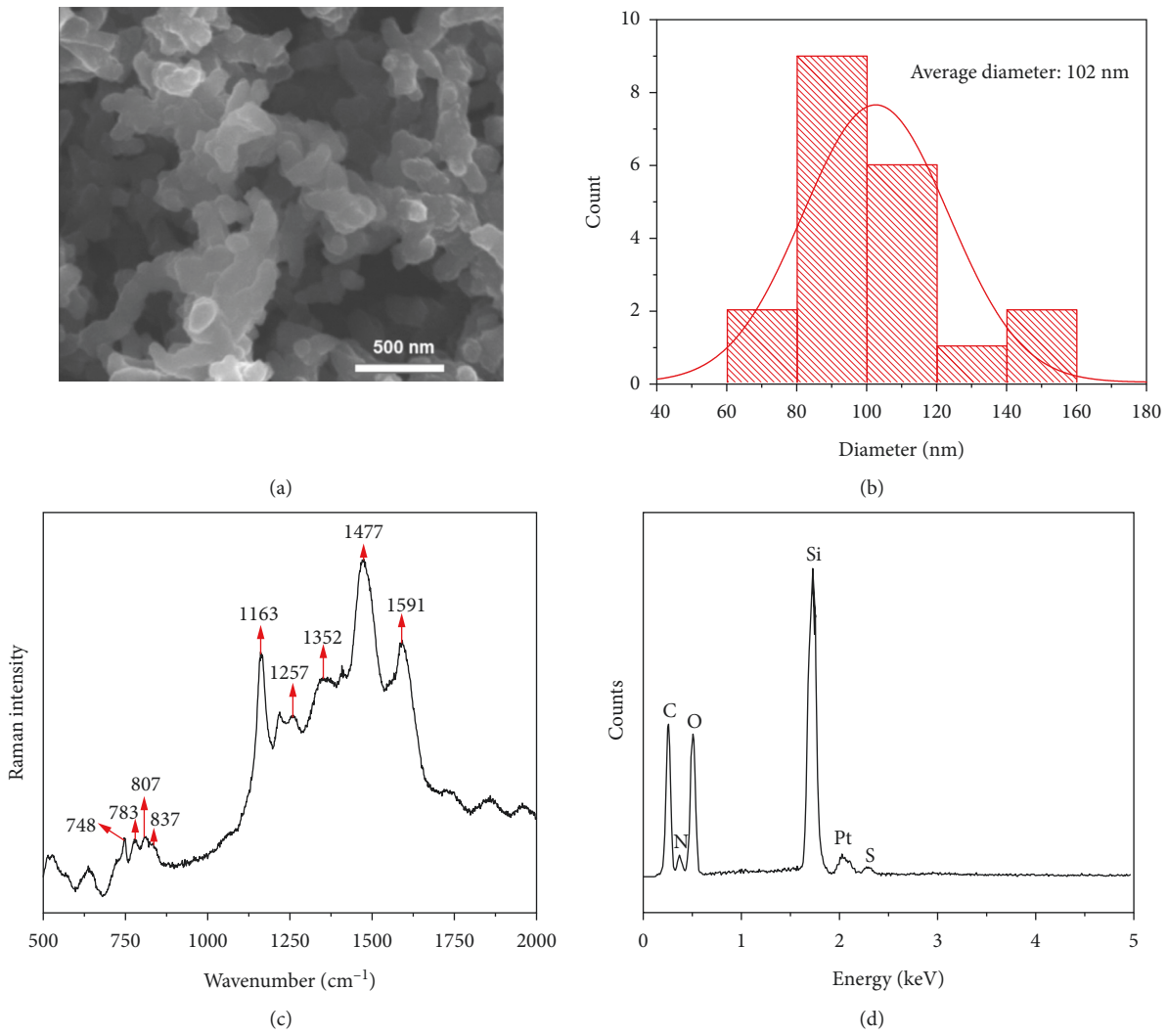

Figure 2: (a) SEM image, (b) nanowire diameter distribution, (c) Raman spectrum, and (d) EDX spectrum of PANi NWs electrosynthesized on Pt WE.

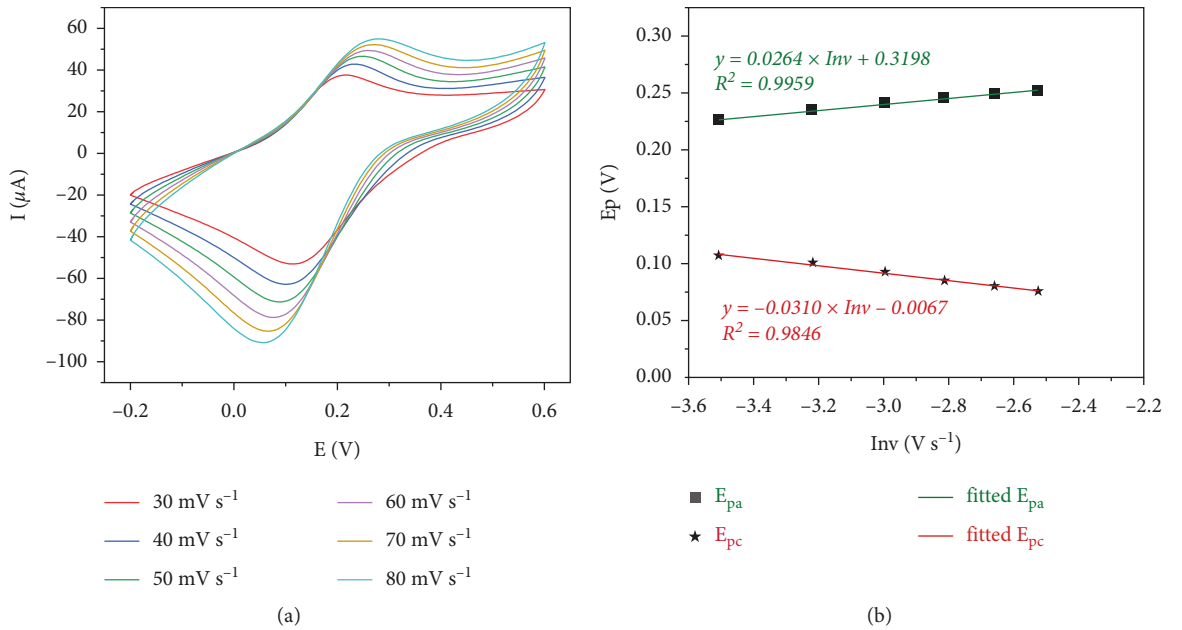

Figure 3: Continued.

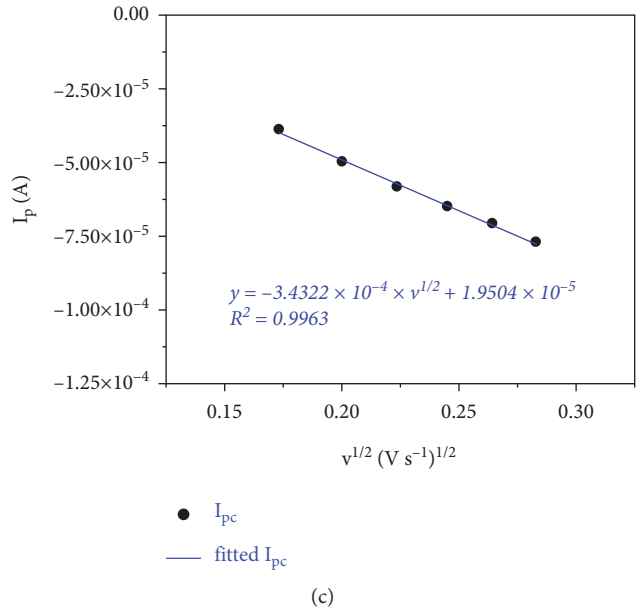

FIGURE 3: (a) CV results of the Pt/PANi NW electrode recorded in $K_3Fe(CN)_6/K_4Fe(CN)_6$ (0.005 M) and 0.1 M KCl solution, at the potential scan rates of 30, 40, 50, 60, 70, and 80 mVs^{-1}; (b) the relationships between the anodic and cathodic peak potentials and lnν and their corresponding linear fit lines: E_{pa}, the green line with square symbols, and E_{pc}, the red line with star symbols; and (c) the relationship between the cathodic peak current (I_{pc}) and the square root of the scan rate ($\nu^{1/2}$) and its corresponding linear fit line.

0.1 M KCl solution (Figure 3(a)). From these CV data, the dependencies of the anodic and cathodic peak potentials on the natural logarithm of the potential scan rate were investigated, and their corresponding linear fit lines for each set of experimental data are shown in Figure 3(b), i.e., E_{pa} vs. lnν,

$$y = 0.0264 \times \ln \nu + 0.3198 \left(R^2 = 0.9959\right), \quad (1)$$

and E_{pc} vs. lnν,

$$y = -0.0310 \times \ln \nu - 0.0067 \left(R^2 = 0.9846\right). \quad (2)$$

It can be seen in Figure 3(b) that the peak potential difference ΔE ($\Delta E = E_{pa} - E_{pc}$) increases as the potential scan rate ν increases. This result indicates that the electrochemical processes happening on the Pt/PANi NW electrode surface are quasireversible [38]. On the other hand, the dependencies of E_{pa} and E_{pc} on lnν in which ν (V s^{-1}) is the potential scan rate are linear, and they are expressed by the following equations [38, 39]:

$$E_{pa} = E^0 + m\left[0.78 + \ln\left(\frac{D^{1/2}}{k^0}\right) - 0.5 \ln m\right] + 0.5m \ln \nu, \quad (3)$$

$$m = \frac{RT}{(1-\alpha)nF}, \quad (4)$$

$$E_{pc} = E^0 - m'\left[0.78 + \ln\left(\frac{D^{1/2}}{k^0}\right) - 0.5 \ln m'\right] - 0.5m' \ln \nu, \quad (5)$$

$$m' = \frac{RT}{\alpha nF}, \quad (6)$$

where $E^0(V)$ is the formal standard potential, α is the charge transfer coefficient, n is the number of transported electrons, k^0 (cm·s^{-1}) is the electron transfer rate constant, D (cm^2·s^{-1}) is the diffusion coefficient, R is the gas constant ($R = 8.314$ J·mol^{-1}·K^{-1}), T is the working temperature ($T = 298$ K), and F is Faraday's constant ($F = 96480$ C·mol^{-1}).

The values of α and n can be calculated from the slopes of E_{pa} vs. lnν and E_{pc} vs. lnν, and the results are that the value of α is 0.460 and the value of n is 0.901. The value of n verifies that the oxidation of $Fe(CN)_6^{4-}$ and the reduction of $Fe(CN)_6^{3-}$ occurring on the Pt/PANi NW electrode surface are through monoelectronic steps. The diffusion coefficients (D_O and D_R) of ferri- and ferrocyanide ions in 0.1 M KCl medium at 25°C are 7.20×10^{-6} cm^2·s^{-1} and 6.66×10^{-6} cm^2·s^{-1}, respectively [40]. From the intercepts of E_{pa} vs. lnν and E_{pc} vs. lnν and $E^0 = (E_{pa} + E_{pc})/2 = 0.17$ V [38], the values of k^0 were calculated as 1.436×10^{-3} cm·s^{-1} and 1.360×10^{-3} cm·s^{-1} for the anodic and the cathodic branches, respectively, and the average value was 1.398×10^{-3} cm·s^{-1}. These results further confirmed that, in the considered scan rate range, the oxidation of $Fe(CN)_6^{4-}$ and the reduction of $Fe(CN)_6^{3-}$ which occurred on the Pt/PANi NW electrode surface are quasireversible.

Besides, from the CV data expressed in Figure 3(a), the relationship between the cathodic peak current and the square root of the potential scan rate is plotted in Figure 3(c):

$$I_{pc} = -3.4322 \times 10^{-4} \times \nu^{1/2} + 1.9504 \times 10^{-5} \left(R^2 = 0.9963\right). \quad (7)$$

It can be seen in Figure 3(c) that the cathodic peak current depends linearly on the square root of the potential scan rate. On the other hand, the electrochemically effective surface area, A (cm^2), of the Pt/PANi NW electrode can be determined by using the Randles–Sevcik equation for quasireversible reactions as follows [41]:

$$I_{pc} = -3.01 \times 10^5 \alpha^{1/2} n^{3/2} A C_0 D^{1/2} \nu^{1/2}, \quad (8)$$

where ν ($V \cdot s^{-1}$), α, n, and D ($cm^2 \cdot s^{-1}$) are mentioned in equations (3)–(6) above, C_0 ($mol \cdot cm^{-3}$) is the concentration of redox species, and I_{pc} (A) is the cathodic peak current. Based on equation (8) and the slope of the linear dependence of the cathodic peak current on the square root of the potential scan rate (Figure 3(c)), the value of A of the Pt/PANi NW electrode was calculated to be 0.147 cm^2. Thus, the electrochemically effective surface area of the Pt/PANi NW WE is nearly 19 times larger than that of the Pt WE (0.785×10^{-2} cm^2).

The above CV, SEM, Raman, and EDX results show that in this work, PANi NWs were formed exactly on a Pt WE with very small area (0.785×10^{-2} cm^2) using the simple and effective CA method. The obtained PANi NWs with one-dimensional nanowire structure and high electrochemically effective surface area will be able to significantly enhance the electrochemical response of the WE and to improve the electrochemical DNA sensor's sensitivity compared with conventional membrane materials [35].

3.2. Direct Immobilization of DNA Probe on Pt/PANi NW Microelectrodes and DNA Hybridization Detection Using PANi NW-Based Electrochemical DNA Sensors. It can be seen in Figure 4 that the R_{ct} value of the Pt/PANi NW/DNA probe electrode (5767 Ω; Figure 4 (curve b)) increases significantly compared to that of the Pt/PANi NW electrode (75 Ω; Figure 4 (curve a)). These results reveal that the immobilization of probe DNA sequences onto the Pt/PANi NW WEs was effectively and simply performed, due to the ability to create links between the amino groups of PANi NWs and the phosphate groups of the probe DNA sequences [42] and due to the PANi nanowire structure with porous surface characteristics and high electrochemically effective surface area.

It can be seen in Figure 5(a) that the impedance values of the DNA sensors after hybridization with different concentrations of complementary target DNA (from 1.0×10^{-13} M to 1.0×10^{-8} M, from curve b to curve g, respectively) increase significantly in comparison with the impedance value of the DNA sensor before hybridization with DNA target (curve a). DNA strands contain negatively charged phosphate groups, while the synthesized PANi NW material is a conducting polymer with p-type charge carriers (holes). Thus, when the DNA hybridization occurred on the sensor surface, the density of the charge carriers of PANi NWs was reduced, leading to the decrease in the conductivity and the increase in the impedance of the sensor.

The R_{ct} value exhibited by a semicircle region at high frequency range on an EIS spectrum depends on changes of

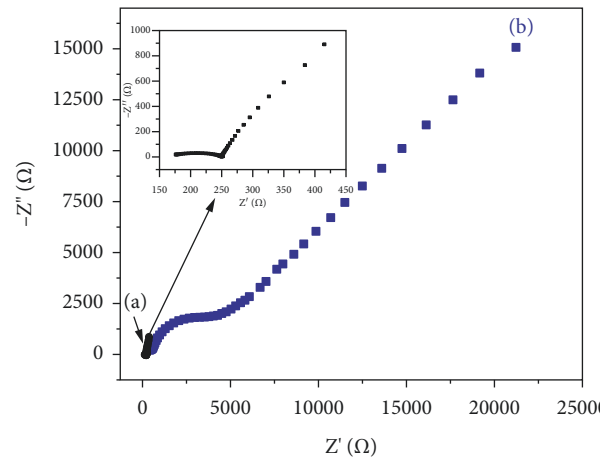

(a) Pt/PANi NW

(b) Pt/PANi NW/DNA probe

Figure 4: EIS spectra (Nyquist plots) of (a) Pt/PANi NWs and (b) Pt/PANi NW/probe DNA microelectrodes measured in PBS buffer (pH 7.4) solution containing $K_3Fe(CN)_6/K_4Fe(CN)_6$ (0.005 M) and 0.1 M KCl, frequency range: 100 kHz–100 mHz, $E_{AC} = 5$ mV, and $E_{DC} = 160$ mV.

the sensor surface where DNA hybridization happens; thus, it is selected as the output signal for DNA target detection. Figure 5(b) (curve a) expresses a good linear relationship between the ΔR_{ct} of the DNA sensor and the logarithm of the complementary DNA target concentration in the range from 1.0×10^{-13} M to 1.0×10^{-8} M. The linear equation is ΔR_{ct} (Ω) = 1891.9448 × $\log C_{\text{DNA target}}$ (M) + 25854.9857 with the correlation coefficient of $R^2 = 0.9916$. The detection limit (LOD) was estimated as 2.48×10^{-14} M (at S/N > 3) [43]. Moreover, as shown in Figure 5(b) (curve b), the response signal at the highest studied concentration (1.0×10^{-8} M) of the noncomplementary target DNA is negligible. The above results indicate that the fabricated DNA sensors using PANi NWs express high sensitivity and good selectivity.

Table 2 exhibits the comparison of the fabricated DNA sensor with some others in the previous studies. The electrochemical DNA sensor based on PANi NWs in this work shows many advantages such as direct detection, high sensitivity, low detection limit (2.48×10^{-14} M), good selectivity, and small volumes of both the DNA probe and DNA target samples (only 5 μL) for the DNA probe immobilization and DNA target detection, respectively. Moreover, the sensor fabrication process proposed in this study is simple and effective with the one-step electrochemical method for the direct synthesis of PANi NWs on the Pt microelectrode's surface, as well as the direct immobilization of DNA probe on the PANi NW material. Therefore, the electrochemical DNA sensor proposed in this study has many potential applications such as detection of pathogenic viruses and bacteria, disease diagnosis, and food safety monitoring. However, similar to the polymerization chain reaction (PCR) techniques, the DNA sensor also works with pretreated biological samples, in which the target DNA sequences need to be extracted before being detected by the Pt/PANi NW microelectrode.

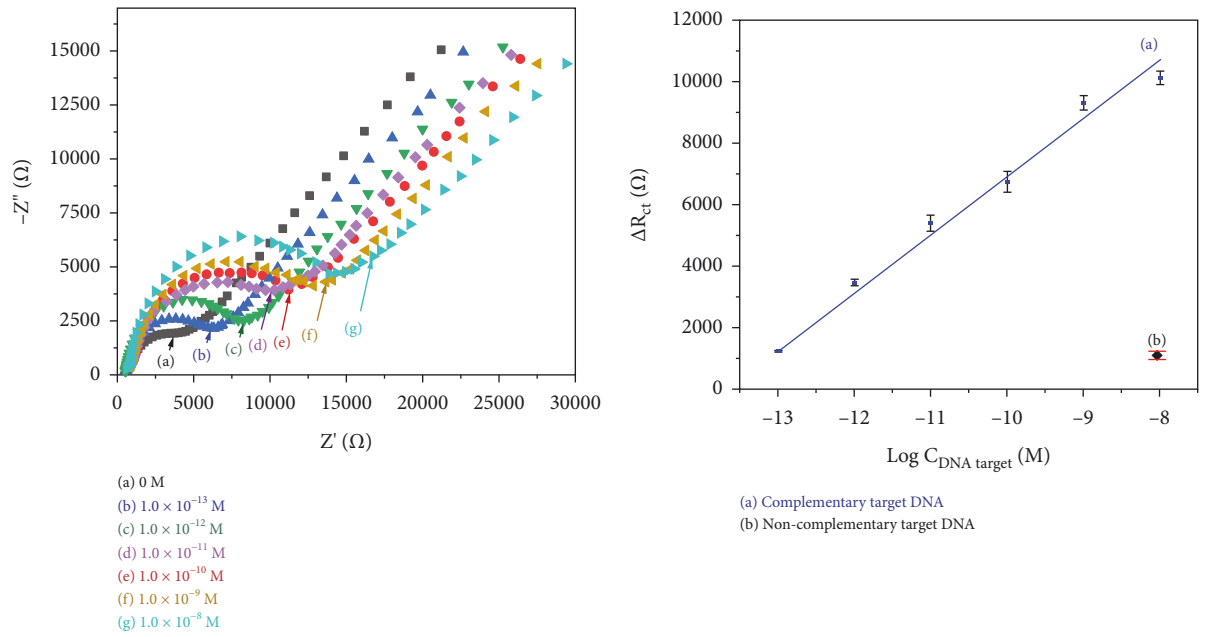

Figure 5: (a) EIS spectra (Nyquist plots) of the DNA sensors after hybridization with different concentrations of complementary target DNA: (a) 0 M, (b) $1.0\times10_{-13}$ M, (c) $1.0\times10_{-12}$ M, (d) $1.0\times10_{-11}$ M, (e) $1.0\times10_{-10}$ M, (f) $1.0\times10_{-9}$ M, and (g) $1.0\times10_{-8}$ M, respectively. Experimental conditions: EIS spectra were measured in PBS buffer (pH 7.4) solution consisting $K_3Fe(CN)_6/K_4Fe(CN)_6$ (0.005 M) and 0.1 M KCl, frequency range: 100 kHz–100 mHz, $E_{AC} = 5$ mV, and $E_{DC} = 160$ mV; and (b) response of the DNA sensors to (a) different concentrations of complementary target DNA and (b) 1.0×10^{-8} M of noncomplementary target DNA.

Table 2: Comparison of this fabricated DNA sensor with some others in the literature.

Surface modification	Synthesis method	Linear range (*M*)	Detection limit (*M*)	Reference
PANi NWs	Three-step electrochemical method	2.25×10^{-12}–2.25×10^{-10}	1.0×10^{-12}	[42]
ERGO/PANi	Drop-casting and electrochemical method	1.0×10^{-13}–1.0×10^{-7}	3.2×10^{-14}	[29]
PANi/graphene sheets	Electrochemical method and drop-casting	1.0×10^{-13}–1.0×10^{-6}	1.0×10^{-14}	[44]
Sm_2O_3 NPs-rGO/PANi	Chemical method and drop-casting	1.0×10^{-13}–1.0×10^{-8}	1.3×10^{-14}	[45]
Graphene sheets-chitosan /PANi/AuNPs	Drop-casting and electrochemical method	1.0×10^{-11}–1.0×10^{-9}	2.11×10^{-12}	[46]
PANi NWs	One-step electrochemical method	1.0×10^{-13}–1.0×10^{-8}	2.48×10^{-14}	This work

4. Conclusion

In this paper, PANi NWs were synthesized directly onto the Pt WEs (with only 0.785 mm^2 area) using the simple one-step electrochemical approach. In particular, the electrochemically effective surface area of the Pt/PANi NW WE is nearly 19 times larger than that of the Pt WE. The Pt/PANi NW microelectrodes with high electrochemically effective surface area, high biocompatibility, and ease of miniaturization facilitated the probe DNA immobilization and enhanced the DNA sensor's electrochemical signals. The detection limit of the sensors was 2.48×10^{-14} M. The DNA sensors exhibited advantages including simple fabrication, direct detection, high sensitivity, good specificity, and easy miniaturization of analytical systems.

Data Availability

The data used to support the findings of this study are included within the article.

Conflicts of Interest

The authors declare that there are no conflicts of interest.

Acknowledgments

This research was funded by Vietnam National Foundation for Science and Technology Development (NAFOSTED) under grant number 104.03-2019.19.

References

[1] A. Mokhtarzadeh, R. Eivazzadeh-Keihan, P. Pashazadeh et al., "Nanomaterial-based biosensors for detection of pathogenic virus," *TRAC Trends in Analytical Chemistry*, vol. 97, pp. 445–457, 2017.

[2] R. Miranda-Castro, R. Sánchez-Salcedo, B. Suárez-Álvarez, N. de-los-Santos-Álvarez, A. J. Miranda-Ordieres, and M. Jesús Lobo-Castañón, "Thioaromatic DNA monolayers for target-amplification-free electrochemical sensing of environmental pathogenic bacteria," *Biosensors and Bioelectronics*, vol. 92, pp. 162–170, 2017.

[3] B. Martín-Fernández, C. L. Manzanares-Palenzuela, M. Sánchez-Paniagua López, N. de-los-Santos-Álvarez, and B. López-Ruiz, "Electrochemical genosensors in food safety assessment," *Critical Reviews in Food Science and Nutrition*, vol. 57, no. 13, pp. 2758–2774, 2017.

[4] J. I. A. Rashid and N. A. Yusof, "The strategies of DNA immobilization and hybridization detection mechanism in the construction of electrochemical DNA sensor: a review," *Sensing and Bio-Sensing Research*, vol. 16, pp. 19–31, 2017.

[5] V. Mani, T. Beduk, W. Khushaim et al., "Electrochemical sensors targeting salivary biomarkers: a comprehensive review," *TRAC Trends in Analytical Chemistry*, vol. 135, Article ID 116164, 2021.

[6] W. Xu, T. Jin, Y. Dai, and C. C. Liu, "Surpassing the detection limit and accuracy of the electrochemical DNA sensor through the application of CRISPR Cas systems," *Biosensors and Bioelectronics*, vol. 155, Article ID 112100, 2020.

[7] N. Wongkaew, M. Simsek, C. Griesche, and A. J. Baeumner, "Functional nanomaterials and nanostructures enhancing electrochemical biosensors and lab-on-a-chip performances: recent progress, applications, and future perspective," *Chemical Reviews*, vol. 119, no. 1, pp. 120–194, 2019.

[8] H. V. Tran, N. D. Nguyen, B. Piro, and L. T. Tran, "Fabrication of a quinone containing layer on gold nanoparticles directed to a label-free and reagentless electrochemical miRNA sensor," *Analytical Methods*, vol. 9, no. 18, pp. 2696–2702, 2017.

[9] J. Li and E.-C. Lee, "Carbon nanotube/polymer composite electrodes for flexible, attachable electrochemical DNA sensors," *Biosensors and Bioelectronics*, vol. 71, pp. 414–419, 2015.

[10] C. S. Y. Yeap, T. Chaibun, S. Y. Lee et al., "Ultrasensitive pathogen detection with a rolling circle amplification-empowered multiplex electrochemical DNA sensor," *Chemical Communications*, vol. 57, no. 91, pp. 12155–12158, 2021.

[11] M. Krečmarová, M. Gulka, T. Vandenryt et al., "A label-free diamond microfluidic DNA sensor based on active nitrogen-vacancy center charge state control," *ACS Applied Materials and Interfaces*, vol. 13, no. 16, pp. 18500–18510, 2021.

[12] L. T. Tran, H. V. Tran, H. T. M. Dang, A. V. Nguyen, T. H. Tran, and C. D. Huynh, "Electrosynthesis of electrochemically reduced graphene oxide/polyaniline nanowire/silver nanoflower nanocomposite for development of a highly sensitive electrochemical DNA sensor," *RSC Advances*, vol. 11, no. 32, pp. 19470–19481, 2021.

[13] M. Lin, H. Wan, J. Zhang, Q. Wang, X. Hu, and F. Xia, "Electrochemical DNA sensors based on MoS_2-AuNPs for polynucleotide kinase activity and inhibition assay," *ACS Applied Materials and Interfaces*, vol. 12, no. 41, pp. 45814–45821, 2020.

[14] K. M. Koo, N. Soda, and M. J. A. Shiddiky, "Magnetic nanomaterial–based electrochemical biosensors for the detection of diverse circulating cancer biomarkers," *Current Opinion in Electrochemistry*, vol. 25, Article ID 100645, 2021.

[15] J. Wang and N. Hui, "Zwitterionic poly (carboxybetaine) functionalized conducting polymer polyaniline nanowires for the electrochemical detection of carcinoembryonic antigen in undiluted blood serum," *Bioelectrochemistry*, vol. 125, pp. 90–96, 2019.

[16] A. I. Inamdar, H. S. Chavan, H. Kim, and H. Im, "Mesoporous Ni-PANI composite electrode for electrochromic energy storage applications," *Solar Energy Materials and Solar Cells*, vol. 201, Article ID 110121, 2019.

[17] E. A. de Oliveira Farias, S. S. Nogueira, A. M. de Oliveira Farias et al., "A thin PANI and carrageenan–gold nanoparticle film on a flexible gold electrode as a conductive and low-cost platform for sensing in a physiological environment," *Journal of Materials Science*, vol. 52, no. 23, pp. 13365–13377, 2017.

[18] E. Saeb and K. Asadpour-Zeynali, "Facile synthesis of TiO_2@PANI@Au nanocomposite as an electrochemical sensor for determination of hydrazine," *Microchemical Journal*, vol. 160, Article ID 105603, 2021.

[19] I. Izwan Misnon and R. Jose, "Charge storage in the PANI–α-MnO_2 polymer–nanocomposite system," *Materials Today Proceedings*, vol. 41, pp. 513–519, 2021.

[20] A. Esmaeeli, A. Ghaffarinejad, A. Zahedi, and O. Vahidi, "Copper oxide-polyaniline nanofiber modified fluorine doped tin oxide (FTO) electrode as non-enzymatic glucose sensor," *Sensors and Actuators B: Chemical*, vol. 266, pp. 294–301, 2018.

[21] N. Hui, X. Sun, S. Niu, and X. Luo, "PEGylated polyaniline nanofibers: antifouling and conducting biomaterial for electrochemical DNA sensing," *ACS Applied Materials and Interfaces*, vol. 9, no. 3, pp. 2914–2923, 2017.

[22] L. T. Tran, H. V. Tran, H. T. M. Dang, C. D. Huynh, and T. A. Mai, "Silver nanoparticles decorated polyaniline nanowires-based electrochemical DNA sensor: two-step electrochemical synthesis," *Journal of the Electrochemical Society*, vol. 167, no. 8, Article ID 087508, 2020.

[23] L. T. Tran, H. V. Tran, T. Tran et al., "A highly sensitive electrochemical DNA sensor based on nanostructured electrode of multi-walled carbon nanotubes/manganese dioxide nano-flowers-like/polyaniline nanowires nanocomposite," *Journal of the Electrochemical Society*, vol. 168, no. 5, Article ID 057518, 2021.

[24] D. Tian, H. Cheng, Q. Li et al., "The ordered polyaniline nanowires wrapped on the polypyrrole nanotubes as electrode materials for electrochemical energy storage," *Electrochimica Acta*, vol. 398, Article ID 139328, 2021.

[25] T. X. Chu, V. P. Vu, H. T. Tran, T. L. Tran, Q. T. Tran, and T. Le Manh, "Molecularly imprinted polyaniline nanowire-based electrochemical biosensor for chloramphenicol detection: a kinetic study of aniline electropolymerization," *Journal of the Electrochemical Society*, vol. 167, no. 2, Article ID 027527, 2020.

[26] K. J. Kshirasagar, U. S. Markad, A. Saha, K. K. K. Sharma, and G. K. Sharma, "Facile synthesis of palladium nanoparticle doped polyaniline nanowires in soft templates for catalytic applications," *Materials Research Express*, vol. 4, no. 2, Article ID 025015, 2017.

[27] T. L. Tran, T. X. Chu, D. C. Huynh, D. T. Pham, T. H. T. Luu, and A. T. Mai, "Effective immobilization of DNA for development of polypyrrole nanowires based biosensor," *Applied Surface Science*, vol. 314, pp. 260–265, 2014.

[28] C. V. Tuan, M. A. Tuan, N. V. Hieu, and T. Trung, "Electrochemical synthesis of polyaniline nanowires on Pt interdigitated microelectrode for room temperature NH_3 gas

sensor application," *Current Applied Physics*, vol. 12, no. 4, pp. 1011–1016, 2012.

[29] M. Du, T. Yang, X. Li, and K. Jiao, "Fabrication of DNA/graphene/polyaniline nanocomplex for label-free voltammetric detection of DNA hybridization," *Talanta*, vol. 88, pp. 439–444, 2012.

[30] R. S. Saberi, S. Shahrokhian, and G. Marrazza, "Amplified electrochemical DNA sensor based on polyaniline film and gold nanoparticles," *Electroanalysis*, vol. 25, no. 6, pp. 1373–1380, 2013.

[31] L. Wang, Q. Yao, H. Bi, F. Huang, Q. Wang, and L. Chen, "PANI/graphene nanocomposite films with high thermoelectric properties by enhanced molecular ordering," *Journal of Materials Chemistry*, vol. 3, no. 13, pp. 7086–7092, 2015.

[32] A. B. Rohom, P. U. Londhe, S. K. Mahapatra, S. K. Kulkarni, and N. B. Chaure, "Electropolymerization of polyaniline thin films," *High Performance Polymers*, vol. 26, no. 6, pp. 641–646, 2014.

[33] H. T. Hien, H. T. Giang, N. V. Hieu, T. Trung, and C. V. Tuan, "Elaboration of Pd-nanoparticle decorated polyaniline films for room temperature NH_3 gas sensors," *Sensors and Actuators B: Chemical*, vol. 249, pp. 348–356, 2017.

[34] G. M. D. Nascimento and M. L. A. Temperini, "Studies on the resonance Raman spectra of polyaniline obtained with near-IR excitation," *Journal of Raman Spectroscopy*, vol. 39, no. 7, pp. 772–778, 2008.

[35] E. Song and J. W. Choi, "Conducting polyaniline nanowire and its applications in chemiresistive sensing," *Nanomaterials*, vol. 3, no. 3, pp. 498–523, 2013.

[36] S. Wang, S. Lu, X. Li, X. Zhang, S. He, and T. He, "Study of H_2SO_4 concentration on properties of H_2SO_4 doped polyaniline counter electrodes for dye-sensitized solar cells," *Journal of Power Sources*, vol. 242, pp. 438–446, 2013.

[37] H. V. Tran, H. T. M. Dang, L. T. Tran, T. V. Chu, and C. D. Huynh, "Metal-organic framework MIL-53(Fe): synthesis, electrochemical characterization, and application in development of a novel and sensitive electrochemical sensor for detection of cadmium ions in aqueous solutions," *Advances in Polymer Technology*, vol. 2020, Article ID 6279278, 10 pages, 2020.

[38] S. Corona-Avendaño, G. Alarcón-Angeles, M. T. Ramírez-Silva, G. Rosquete-Pina, M. Romero-Romo, and M. Palomar-Pardavé, "On the electrochemistry of dopamine in aqueous solution. part I: the role of [SDS] on the voltammetric behavior of dopamine on a carbon paste electrode," *Journal of Electroanalytical Chemistry*, vol. 609, no. 1, pp. 17–26, 2007.

[39] J. Li, L. He, J. Jiang et al., "Facile syntheses of bimetallic prussian blue analogues ($K_xM[Fe(CN)_6]\cdot nH_2O$, M=Ni, Co, and Mn) for electrochemical determination of toxic 2-nitrophenol," *Electrochimica Acta*, vol. 353, Article ID 136579, 2020.

[40] S. J. Konopka and B. McDuffie, "Diffusion coefficients of ferri- and ferrocyanide ions in aqueous media, using twin-electrode thin-layer electrochemistry," *Analytical Chemistry*, vol. 42, no. 14, pp. 1741–1746, 1970.

[41] J. Krejci, Z. Sajdlova, V. Nedela et al., "Effective surface area of electrochemical sensors," *Journal of the Electrochemical Society*, vol. 161, no. 6, pp. B147–B150, 2014.

[42] N. Zhu, Z. Chang, P. He, and Y. Fang, "Electrochemically fabricated polyaniline nanowire-modified electrode for voltammetric detection of DNA hybridization," *Electrochimica Acta*, vol. 51, no. 18, pp. 3758–3762, 2006.

[43] H. V. Tran, B. Piro, S. Reisberg, L. D. Tran, H. T. Duc, and M. C. Pham, "Label-free and reagentless electrochemical detection of microRNAs using a conducting polymer nanostructured by carbon nanotubes: application to prostate cancer biomarker miR-141," *Biosensors and Bioelectronics*, vol. 49, pp. 164–169, 2013.

[44] Q. Zheng, H. Wu, Z. Shen et al., "An electrochemical DNA sensor based on polyaniline/graphene: high sensitivity to DNA sequences in a wide range," *Analyst*, vol. 140, no. 19, pp. 6660–6670, 2015.

[45] N. Mohammadian and F. Faridbod, "ALS genosensing using DNA-hybridization electrochemical biosensor based on label-free immobilization of ssDNA on Sm_2O_3 NPs-rGO/PANI composite," *Sensors and Actuators B: Chemical*, vol. 275, pp. 432–438, 2018.

[46] L. Wang, E. Hua, M. Liang et al., "Graphene sheets, polyaniline and AuNPs based DNA sensor for electrochemical determination of BCR/ABL fusion gene with functional hairpin probe," *Biosensors and Bioelectronics*, vol. 51, pp. 201–207, 2014.